J. Fluid Mech. (2006), *vol.* 552, *pp.* 1–11.
doi:10.1017/S002211200500772X Printed in the United Kingdom

The front speed of intrusive gravity currents

By H.-B. CHEONG[1], J. J. P. KUENEN[2] AND P. F. LINDEN[3]

[1]Department of Environmental Atmospheric Sciences, Pukyong National University, 599-1 Daeyeon-3-dong, Nam-gu, Pusan 608-737, Korea

[2]Department of Applied Physics, Eindhoven University of Technology, P. O. Box 513, 5600 MB Eindhoven, The Netherlands

[3]Department of Mechanical and Aerospace Engineering, University of California, San Diego, 9500 Gilman Drive, La Jolla, CA 92093-0411, USA

(Received 14 June 2005 and in revised form 10 August 2005)

This paper describes an experimental and numerical study of an intrusion propagating along the interface of a two-layer fluid in a channel. We find that when the density of the intrusion is the depth-weighted mean of the layer densities the interface ahead of the intrusion is undisturbed, but for other densities the interface ahead of the intrusion is displaced vertically. We find that this vertical displacement, which takes the form of an upstream-propagating long wave, depends on the properties of the intrusion and not only on the relative depths of the two layers. For the case when the interface is undisturbed the intrusion propagation speed is a minimum. We develop an energy argument that describes the observed variation of the intrusion speed from this minimum speed as a function of the intrusion and layer densities and the ratio of the layer depths. We also show that if, and only if, the layer depths are equal, the speed of the intrusion is independent of the density of the intrusion.

1. Introduction

An intrusive gravity current (IGC) forms when fluid of one density travels along an interface between two layers of different densities†. An IGC can be created in the laboratory using a simple lock release (figure 1) where the density ρ_i of the fluid in the intrusion is greater than the density ρ_U of the upper-layer fluid and smaller than the density ρ_L of the lower-layer fluid. When the lock gate is removed, the fluid behind the lock travels as an IGC along the interface of the two fluid layers, driven by the buoyancy forces.

The first theoretical description of a high-Reynolds-number IGC used a hydraulic approach, in the spirit of Benjamin's (1968) analysis of a gravity current, in which mass, momentum and energy are conserved in a control volume moving with the speed of the current, and the interface ahead of the intrusion is assumed to be undisturbed (Holyer & Huppert 1980). The cubic governing equation has three possible solutions, which were compared with three experiments carried out by Dr J. E. Simpson. It was found that the solution corresponding to the maximum IGC volume flux gave approximate agreement with the observed speeds.

† An IGC will also form if the layers are stratified or if the ambient fluid is continuously stratified. However, here we restrict attention to the simpler case where the effects of stratification are confined to a single sharp interface.

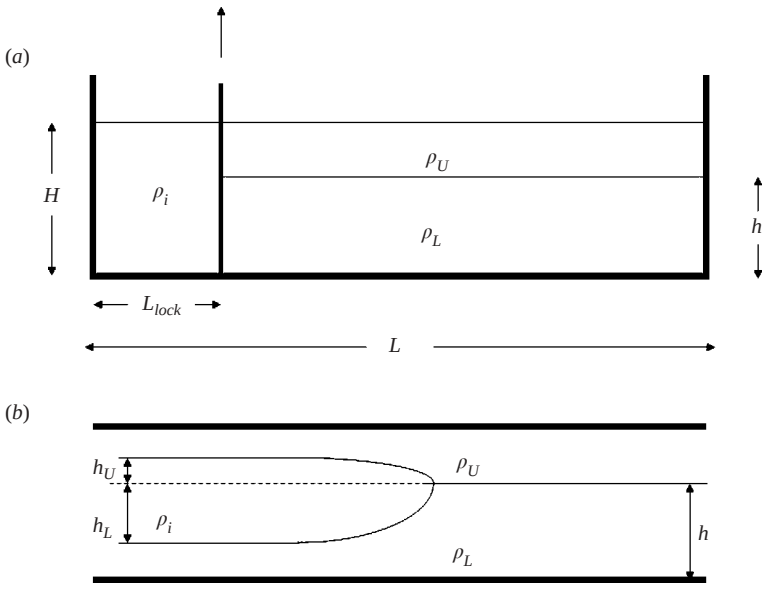

FIGURE 1. (*a*) Schematic view of the initial situation for the intrusive gravity current, where $\rho_U < \rho_i < \rho_L$ and $0 < h < H$. (*b*) A sketch of the intrusion for the case where the equilibrium depth (1.3) $\hat{h}_E < 0.5$.

Lock-release experiments on the doubly symmetrical case, where $\rho_i = \frac{1}{2}(\rho_U + \rho_L)$ and $h = \frac{1}{2}H$, were carried out by Britter & Simpson (1981). They showed that, in this case, the interface ahead of the current remained flat and that the IGC propagated at a constant speed for several lock lengths. Further experiments on the doubly symmetric IGC at large Reynolds numbers showed that it can be considered as a gravity current in one layer and its mirror image in the plane of the interface in the other layer (Lowe, Linden & Rottman 2002). The measurements of the propagation speed and the shape of the intrusion were in agreement with Benjamin's (1968) energy-conserving theory for gravity currents.

Experiments with equal layer depths, but with the IGC density no longer restricted to be the average of the layer densities, were carried out by de Rooij, Linden & Dalziel (1999). They found that relatively dense or light intrusions generated large-amplitude interfacial waves ahead of the intrusion, which caused vertical displacements of the interface. Sutherland, Kyba & Flynn (2004) reworked Holyer & Huppert's (1980) theory, specializing it for the Boussinesq case. They developed a perturbation solution for small departures from the doubly symmetric case, again assuming that the interface was undisturbed ahead of the IGC. In experiments in which they varied the densities and layer depths, the measured intrusion speeds were about 5–10% lower than their perturbation theory predicted. They also observed significant interfacial wave generation ahead of the IGC when the density of the intrusion was not the depth-weighted mean of the layer densities, and noted that the exact theory of Holyer & Huppert (1980) significantly underpredicts the intrusion speeds in that case. They attributed this discrepancy to the generation of the interfacial waves.

Except for the doubly symmetric IGC, the theories that assume the interface is undisturbed give poor agreement with experiments and the role of the interfacial waves in the dynamics and propagation of an IGC remains unclear. We will show that

it is essential to consider the vertical displacement of the interface in the discussion of the intrusion dynamics.

In the special case when $h=0$, the flow corresponds to a dense gravity current propagating along the bottom boundary underneath a uniform less-dense fluid. In the early stages of a lock release the current is observed to travel at a constant speed U_0 (Rottman & Simpson 1983), and dimensional analysis predicts that the front speed for a Boussinesq current takes the form

$$U_0 = F\sqrt{g'_{iU}H}, \tag{1.1}$$

where $g'_{iU} \equiv g(\rho_i - \rho_U)/\rho_0$ is the reduced gravity (g is the acceleration due to gravity) of the IGC relative to the upper layer and ρ_0 is a representative density. The Froude number F is, in general, a function of Reynolds number $Re = \sqrt{g'_{iU}H^3}/\nu$, where ν is the kinematic viscosity, but as Re increases the Froude number becomes less dependent on Reynolds number (Keulegan 1958; Barr 1967). In the ideal case, where the Reynolds number is infinite, bottom friction is ignored and energy is conserved, Benjamin (1968) showed that $F=1/2$. Experiments on gravity currents which include bottom stress and some dissipation give values of about $F=0.48$ at high Reynolds numbers (Shin, Dalziel & Linden 2004). Similarly, we can consider the case of $h=H$ as that of a less dense current propagating with speed U_H at the surface of a dense fluid.

We non-dimensionalize speeds by the speed $\sqrt{g'_{LU}H}$ of long waves on the interface, where $g'_{LU} \equiv g(\rho_L - \rho_U)/\rho_0$ is the reduced gravity of the interface, and depths by H. Dimensionless variables are denoted by a hat. We refer to the case where the density of the intrusion is equal to the depth-weighted mean density

$$\rho_i = \frac{h\rho_L + (H-h)\rho_U}{H}, \tag{1.2}$$

as the equilibrium IGC and denote the corresponding interface height (the solution of (1.2) for given densities) as the equilibrium height h_E. In terms of the reduced gravities, the equilibrium depth, from (1.2), is given by

$$\hat{h}_E \equiv \frac{h_E}{H} = \frac{g'_{iU}}{g'_{LU}}. \tag{1.3}$$

Thus the two limiting cases, the bottom and the surface gravity currents, have dimensionless speeds

$$\hat{U}_0 = F\sqrt{\frac{g'_{iU}}{g'_{LU}}} = F\sqrt{\hat{h}_E} \quad \text{and} \quad \hat{U}_H = F\sqrt{\frac{g'_{Li}}{g'_{LU}}} = F\sqrt{(1-\hat{h}_E)}, \tag{1.4}$$

where $g'_{Li} \equiv g(\rho_L - \rho_i)/\rho_0$ is the reduced gravity between the lower layer and the lock fluid.

Since there is no deflection of the interface for the equilibrium IGC, it may be considered as a combination of an upper and lower gravity current, in the manner of the doubly symmetric case, in each layer. Thus the normalized speed of the equilibrium IGC is

$$\hat{U}_E = F\sqrt{\frac{g'_{Li}}{g'_{LU}}\frac{h_E}{H}} = F\sqrt{\frac{g'_{iU}}{g'_{LU}}\left(1-\frac{h_E}{H}\right)} = F\sqrt{\hat{h}_E(1-\hat{h}_E)}. \tag{1.5}$$

Comparison of (1.4) with (1.5) shows that $\hat{U}_0 > \hat{U}_E$ and $\hat{U}_H > \hat{U}_E$, so that the equilibrium IGC travels more slowly than the surface and bottom gravity currents.

The purpose of this paper is to determine the speeds of an IGC for a range of density differences and depth ratios, and to investigate the role of interfacial waves and the interfacial displacement. The paper is organized as follows. The experiments and numerics are described in § 2, and the results are discussed in § 3. An explanation of the results in terms of the energetics of the flows is given in § 4 and the conclusions are given in § 5.

2. Experiments and numerics

2.1. *Experimental method*

The tank was $L = 182$ cm long, 23 cm wide and 30 cm deep. For all experiments the total fluid height $H = 20$ cm and the gate was positioned at $L_{lock} = 30$ cm from the end wall (figure 1*a*). Thus the intrusions propagated about 5 lock lengths and so were expected, and observed, to travel at constant speeds after the initial acceleration from rest. The flow was recorded with a CCD camera, connected to a PC for image analysis, and positioned 3.4 m in front of the tank. The back of the tank was covered with tracing film and illuminated with two 95 W fluorescent lamps.

The tank was first filled with a salt solution, of density ρ_L and dyed with green food colour, to the required height h. A layer of fresh water with density ρ_U was carefully floated on top, until the total height $H = 20$ cm. Then the gate was pushed down and the fluid behind the gate was stirred. To obtain the desired density ρ_i, salt was added to the lock, or solution was removed and replaced by an equal amount of fresh water. Potassium permanganate was used to colour this fluid. Densities were measured using an Anton Paar DMA 5000 density meter to a precision of 10^{-5} g ml^{-1}. Density differences were less than 1.5%, so that the flows were Boussinesq.

The experiment was started by pulling the gate vertically out of the tank. The flow images were captured by the camera every 1/24 s, and analysed using DigiFlow (Dalziel 2004). The attenuation of light passing through the tank was used to determine the density field in the flow. From this density field, the cross-tank mean density, integrated vertically in the z-direction, was calculated for every x-position and time t. The front speed of the intrusive gravity current was calculated from the resulting x–t plot (for further details of this method see Shin *et al.* 2004).

Initially, three series, A, B and C, of experiments were performed, each with different fixed values of the densities ρ_L, ρ_U and ρ_i. These had equilibrium depths $h_E > H/2$, $h_E = H/2$ and $h_E < H/2$, respectively. In each series the interface height h was varied between its extreme values $h = 0$ and $h = H$. Table 1 gives the parameters of the experiments and the measured front speeds. We also carried out six experiments to examine the vertical displacement of the interface ahead of the IGC (figures 3 and 4).

After we developed the theory for the speed of the IGC (see (4.6)) we noted that the theory predicts that, when the two layers have equal depths, the speed of the intrusion is independent of the density of the intrusion (provided it is between the densities of the two layers). We then carried out additional experiments with equal layer depths to test this result. In that case the flow was visualized using a shadowgraph, and the front of the intrusion was timed between two locations 50 cm apart. The parameters are given in table 2.

2.2. *Numerical method*

The governing equations are the two-dimensional Boussinesq equations with vorticity and density as prognostic variables. These equations are given in (13)–(15) in

Series	$\hat{h}$	0	0.1	0.2	0.3	0.4	0.5	0.6	0.7	0.8	0.9	1.0
A												
$\hat{U}_h$	Exp.	0.37	0.38	0.32	–	–	0.25	–	–	0.26	0.28	0.28
$\hat{U}_h$	Num.	0.38	0.36	0.31	0.27	0.25	0.25	0.24	0.24	0.26	0.28	0.31
B												
$\hat{U}_h$	Exp.	0.33	0.33	–	–	–	0.26	–	–	–	0.34	0.33
$\hat{U}_h$	Num.	0.35	0.32	0.29	0.26	0.25	0.25	0.25	0.26	0.29	0.32	0.35
C												
$\hat{U}_h$	Exp.	0.24	–	0.23	–	–	0.24	–	0.34	–	–	0.43
$\hat{U}_h$	Num.	0.25	0.23	0.22	0.21	0.22	0.23	0.25	0.29	0.33	0.39	0.42

TABLE 1. The dimensionless speeds as measured in the experiments and the numerics. Series A: $\rho_L = 1.0064\,\mathrm{g\,ml^{-1}}$, $\rho_i = 1.0032\,\mathrm{g\,ml^{-1}}$, $\hat{h}_E = 0.61$. Series B: $\rho_L = 1.0046\,\mathrm{g\,ml^{-1}}$, $\rho_i = 1.0014$ g ml^{-1}, $\hat{h}_E = 0.50$. Series C: $\rho_L = 1.0046\,\mathrm{g\,ml^{-1}}$, $\rho_i = 0.9998\,\mathrm{g\,ml^{-1}}$, $\hat{h}_E = 0.25$. In each case $\rho_U = 0.9982\,\mathrm{g\,ml^{-1}}$.

ρ_L	1.0064	1.0046	1.0046	1.0107	1.0110	1.0112	1.0113	1.0108	1.0109	1.0061	1.0058
ρ_U	0.9982	0.9982	0.9982	0.9987	0.9987	0.9987	0.9987	0.9987	0.9987	0.9988	0.9988
ρ_i	1.0032	1.0014	0.9998	1.0051	1.0086	1.0082	1.0038	1.0024	1.0030	1.0025	1.0016
$\hat{U}_h$	0.25	0.26	0.24	0.25	0.22	0.23	0.23	0.23	0.23	0.25	0.24

TABLE 2. Densities (g ml^{-1}) and measured dimensionless velocities for experiments with two layers of equal depths.

Härtel, Meiburg & Necker (2000). The viscosity ($1 \times 10^{-2}\,\mathrm{cm^2\,s^{-1}}$) and diffusivity ($1.5 \times 10^{-5}\,\mathrm{cm^2\,s^{-1}}$) appropriate for salt water were used. Zero-flux boundary conditions were imposed on the density field at all boundaries. The velocity field satisfied no-normal flow and no-slip conditions at the boundaries, except at the bottom boundary where either a slip or no-slip condition is applied. Initially, the fluid was at rest, and domain was stratified as in figure 1(*a*), using the same values of the density as in table 1. The density variation across the interface was given by a smooth function, and the interface thickness was less than $0.05H$. The equations were discretized using spectral transforms in space (Catuno *et al.* 1988) and the leap-frog method in time. For the no-slip boundary condition, the vorticity at the bottom was modified based on the finite-difference analogue (Weinan & Liu 1996). The numerical domain was the same size as the experimental tank and had 1024 and 256 grid points in the horizontal and vertical directions, respectively. With this grid spacing the front speed of the IGC was found to be insensitive to the resolution. We compared the front speed of the bottom-propagating gravity current in case of a slip bottom with the numerical result of Härtel *et al.* (2000). The front speed, at a very high Reynolds number (of order 10^5), was $0.967U_0$, taking $F = 0.5$ in (1.1), while the front speed calculated by Härtel *et al.* (2000) was $0.977U_0$. This is very good agreement in spite of different numerical approaches.

3. Results

Figure 2 shows images taken from the experiments and the corresponding numerical simulations for $\hat{h}_E = 0.25$, for a range of dimensionless interface heights $\hat{h} = 0$, 0.25,

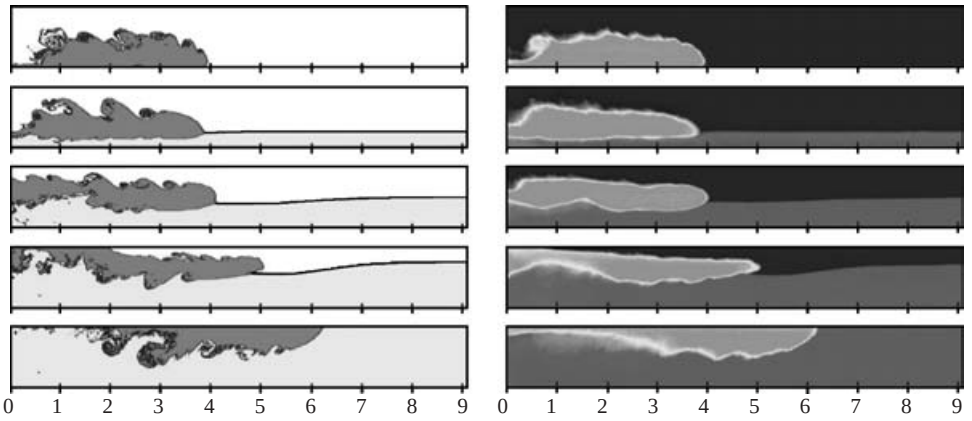

FIGURE 2. Snapshots at $t = 20$ s of intrusive gravity currents produced by the simulation and experiment for Series C. Parameters are $\hat{h}_E = 0.25$, $\sqrt{g'_{LU}H} = 11.2\,\mathrm{cm\,s^{-1}}$ and $Re = 22\,400$. The length is scaled by the total depth H. The numerical simulations are shown in the left panels and the experiments in the right panels. From the upper to lower panels, the dimensionless interface height $\hat{h}$ is 0, 0.25, 0.50, 0.75, and 1, respectively.

0.50, 0.75 and 1. There is excellent agreement between the experiments and the calculations, both in the speed of propagation as given by the location of the front and also in the qualitative features of the flow. The simulations show larger billow structures than are observed in the experiments, and this is due to the restriction to two dimensions in the calculations. In practice these are broken down by three-dimensional instabilities (Härtel *et al.* 2000). The second panel from the top is the equilibrium case and we observe, as expected, that the interface ahead of the intrusion is flat. For $\hat{h}_E = 0.50$ and 0.75, there is a wave of depression, which is larger in the latter case which is further from the equilibrium height. In these latter cases the intrusion is less dense than the mean-depth weighted density and the IGC flows above the undisturbed interface height.

Images from the six experiments which examine the displacement of the interface are shown in figure 3. We see that the interface is elevated when $\hat{h} < \hat{h}_E$ and depressed when $\hat{h} > \hat{h}_E$. Note, particularly, that this occurs irrespective of the depth of the interface. For example, for $\hat{h} = 0.75$ the interface both falls (figure 4*c*, *d*) and rises figure 4*f*. Hence, the motion of the interface is not always in the direction towards the deeper layer. The magnitude of the deflection $\delta\hat{h}$ is plotted against $\hat{h}_E - \hat{h}$ in figure 4. The data fit a least-squares straight line $\delta\hat{h} = 0.30(\hat{h}_E - \hat{h})$, with an uncertainty in the coefficient of about 0.02.

In figure 5(*a*–*c*) the dimensionless front speed $\hat{U}$ is plotted against the dimensionless interface height $\hat{h}$ for each of the three density configurations. The experimental error in the front speed is about 10%. The numerical results for the front speeds are also plotted on these figures and they show very good agreement with the experimental results.

4. An energy model

The IGC results from a release of potential energy stored in the original lock configuration. After it travels along the interface and all the motion has ceased, the intrusion eventually leaves three layers. If the layers are formed without any mixing

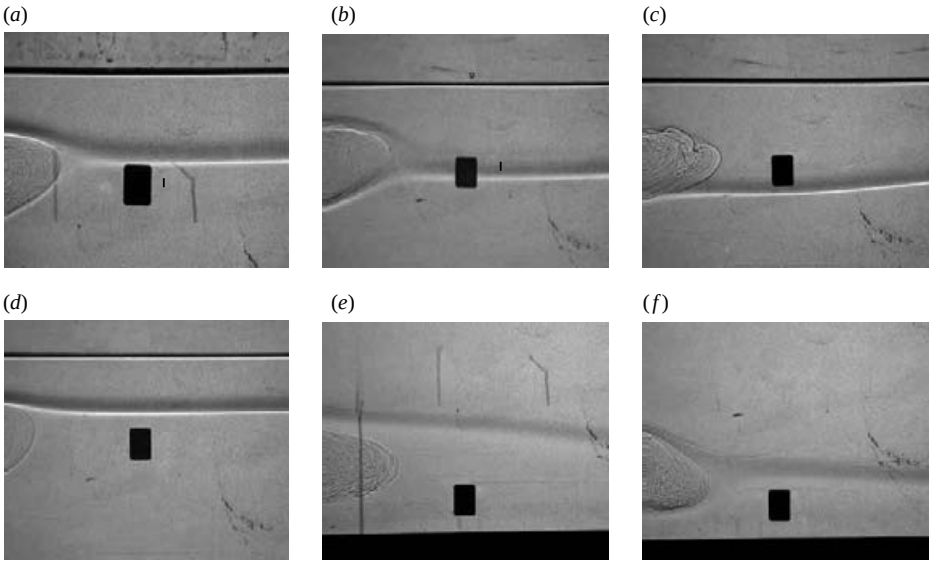

FIGURE 3. Shadowgraph images showing the deflection of the interface caused by the intrusion. (*a*) $\hat{h}=0.75$, $\hat{h}_E=0.76$, (*b*) $\hat{h}=0.75$, $\hat{h}_E=0.44$, (*c*) $\hat{h}=0.75$, $\hat{h}_E=0.29$, (*d*) $\hat{h}=0.75$, $\hat{h}_E=0.89$, (*e*) $\hat{h}=0.25$, $\hat{h}_E=0.77$, (*f*) $\hat{h}=0.25$, $\hat{h}_E=0.35$. The initial interface height coincides with the top of the black rectangle.

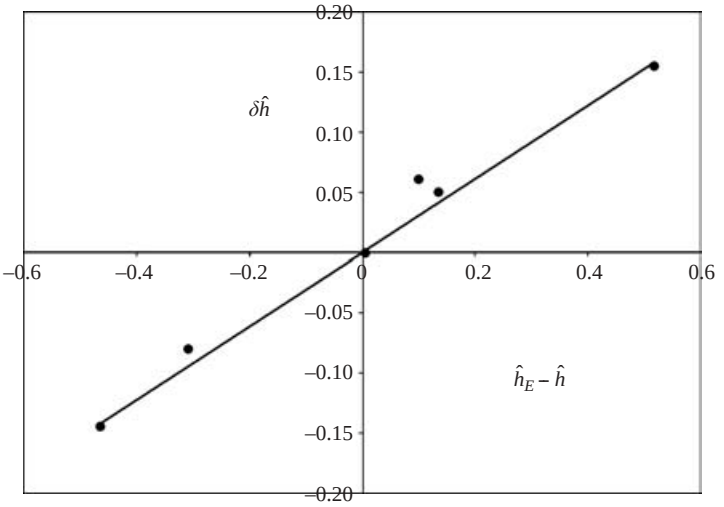

FIGURE 4. The dimensionless interface deflection $\delta\hat{h}$ plotted against the departure $\hat{h}_E-\hat{h}$ from the equilibrium IGC. The straight line is the least squares linear fit $\delta\hat{h}=0.30(\hat{h}_E-\hat{h})$.

their thicknesses from the bottom to the surface are $(1-\alpha)h$, αH and $(1-\alpha)(H-h)$, respectively, where $\alpha=L_{lock}/L$. The available potential energy (APE) ΔP, per unit length of the channel, defined as the difference in potential energy between the initial and final state, is readily calculated as

$$\Delta P=\tfrac{1}{2}g\alpha(1-\alpha)(h^2\rho_L+(H^2-2hH)\rho_i+(H^2+2hH-h^2)\rho_U). \tag{4.1}$$

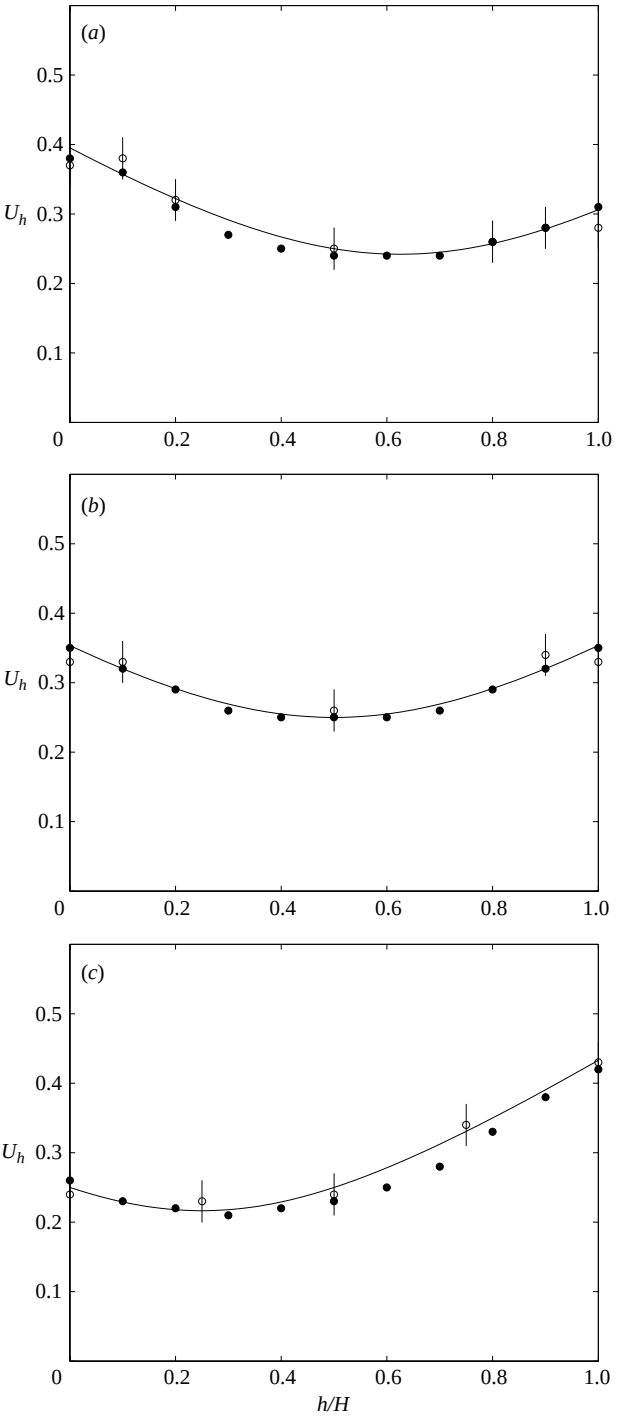

FIGURE 5. Plots of the dimensionless front speed $\hat{U}_h$ as a function of dimensionless interface height $\hat{h}$ for Series A–C, a–c respectively. The open circles are the experimental results and the closed circles are the numerical results. The curve in each graph is the theoretical prediction (4.6). The error bars represent the uncertainty in the experimental measurements.

The minimum value of this APE occurs when $\mathrm{d}\Delta P/\mathrm{d}h = 0$, i.e. when

$$h(\rho_L - \rho_U) = H(\rho_i - \rho_U), \tag{4.2}$$

which is satisfied by the equilibrium depth $h = h_E$ (see (1.2)).

Alternatively, we can calculate the APE per unit area, E, due to the horizontal density difference, taking the interface as the reference level, as

$$E = g\int_{-h}^{0}(\rho_L - \rho_i)z\,\mathrm{d}z + g\int_{0}^{H-h}(\rho_i - \rho_U)z\,\mathrm{d}z \tag{4.3}$$

$$= \tfrac{1}{2}g(\rho_L - \rho_i)h^2 + \tfrac{1}{2}g(\rho_i - \rho_U)(H-h)^2. \tag{4.4}$$

It is easily seen that the equilibrium depth given by (4.2) implies that $\mathrm{d}E/\mathrm{d}h = 0$, so that this APE is also a minimum for this depth. Departures from the minimum value of the APE are quadratic in $h - h_E$, the distance of the interface from the equilibrium height.

As many have pointed out since the pioneering work of Yih (1965), the kinetic energy of gravity currents and intrusions comes from the conversion of the APE as the density field adjusts. Indeed, theories of gravity currents (e.g. Benjamin 1968; Shin *et al.* 2004) have assumed that this conversion occurs without any losses. In this spirit, we assume that the variation of the IGC speed from its equilibrium value can be expressed in terms of this energy balance. Hence, we write

$$\hat{U}_h^2 = \hat{U}_E^2(a(\hat{h} - \hat{h}_E)^2 + b(\hat{h} - \hat{h}_E) + c). \tag{4.5}$$

The parameters a, b and c can be determined using the results of the three special cases, $\hat{h} = 0$, $\hat{h} = \hat{h}_E$ and $\hat{h} = 1$. Applying these limits, and using (1.5) and (1.4), gives $a = 1/(h_E(1-h_E))$, $b = 0$ and $c = 1$. Hence

$$\hat{U}_h = F\sqrt{\hat{h}^2 - 2\hat{h}\hat{h}_E + \hat{h}_E}. \tag{4.6}$$

This curve is plotted on figure 5(*a–c*) for each series of experiments, and it agrees with the experimental data within the experimental error and with the numerical results. Given that this model assumes that the interface has zero thickness and ignores any energy losses due to mixing or friction, this agreement suggests that the first-order dynamics are captured by this analysis.

An interesting feature of (4.6) is found for the case where the two layers have equal depths, $\hat{h} = 0.5$. In this case $\hat{U}_h = \frac{1}{2}F$, and (4.6) predicts that the speed of the IGC is independent of the equilibrium height $\hat{h}_E$. This means that the speed of the intrusion is, in this case, the same for all values of the lock density, $\rho_U < \rho_i < \rho_L$. We were surprised by this prediction and subsequently carried out a series of experiments to test this result (table 2). The results of these experiments are shown in figure 6. If we take $F = \frac{1}{2}$ (Benjamin 1968) then $\hat{U}_h = 0.25$, shown as the dashed line in figure 6, and the experiments conform to the prediction.

Finally, we return to the role of the interfacial wave ahead of the intrusion. We observed, as did Sutherland *et al.* (2004), that the interface in front of the intrusion remained undisturbed when the intrusion density was equal to the depth-weighted mean density (i.e. it corresponded to the equilibrium IGC). The reason for this result is that, since the IGC flows at its neutral depth (e.g. it sinks down if it is heavier than the mean of the densities of the two layers), it satisfies

$$g'_{iU}h_U = g'_{Li}h_L. \tag{4.7}$$

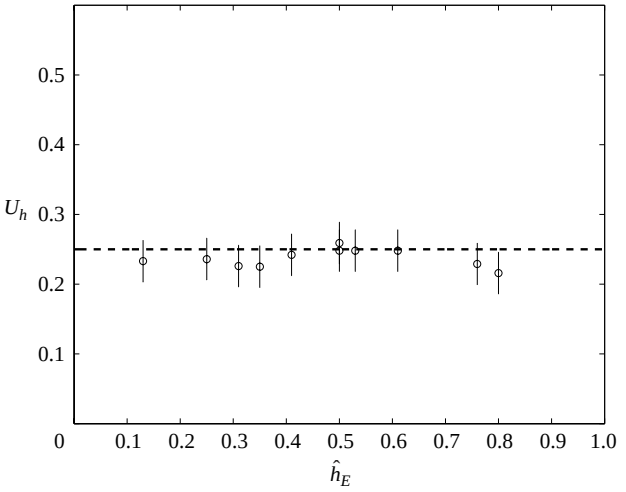

FIGURE 6. $\hat{U}_h$ plotted against the dimensionless intrusion density $(\rho_i - \rho_U)/(\rho_L - \rho_U) \equiv \hat{h}_E$. The dashed line is $\hat{U}_h = \frac{1}{2}F$, with $F = 0.5$.

Application of mass, momentum and energy conservation (de Rooij *et al.* 1999) shows that, when the interface ahead of the intrusion remains undisturbed, the front speeds in each layer are related to the downstream intrusion heights h_U and h_L by

$$U_U = \sqrt{2g'_{iU}h_U}\left(1 - \frac{h_U}{H-h}\right) \text{ and } U_L = \sqrt{2g'_{Li}h_L}\left(1 - \frac{h_L}{h}\right), \tag{4.8}$$

respectively, where we denote the lower and upper layer speeds by U_L and U_U, respectively (figure 1*b*). Since these two speeds must be equal, (4.7) and (4.8) imply that $h_U/(H-h) = h_L/h$, and a little algebra shows that this requires $\hat{h} = \hat{h}_E$. Thus a fully consistent solution with no upstream disturbance of the interface is possible in this case.

Further, (4.8) implies that $U_U > U_L$ when $\hat{h} < \hat{h}_E$, and vice-versa. Since this inequality in speeds is impossible, the interface ahead of the IGC must adjust to compensate for this difference in speeds. If we imagine the two parts of the intrusions as gravity currents, when $U_U > U_L$ the interface will rise, and vice-versa. This behaviour is consistent with the observations in figures 3 and 4, and we find that the magnitude of the interface deflection is proportional to the departure from the equilibrium case.

5. Conclusions

We have shown that the interface ahead of an IGC remains undisturbed only in the special case when the intrusion density is the depth-weighted mean of the layer densities. In other cases the interface is either elevated or depressed by a long wave that propagates ahead of the IGC. This wave appears to be generated by the gravitational adjustment of the lock fluid when the gate is removed. Previous hydraulic theories that ignore this adjustment and the consequent deflection of the interface are unable to predict the propagation speed of the intrusion. We provide a new description of the speed of an IGC, propagating along a sharp density interface at high Reynolds number, in terms of the conversion of available potential energy into kinetic energy. Our experimental and numerical results agree with the predicted speeds, within a few percent. This theory predicts that, in the special case when the

two layers have equal depth, the speed of the IGC is independent of the density of the intrusion. This prediction is consistent with our experiments.

This problem was first suggested to P. F. L. when he started his PhD in 1969 by Stewart Turner, showing that Stewart is a scientist far ahead of his time.

This work was carried out while H. B. C. and J. J. P. K. were visiting the MAE department at UCSD. H. B. C. was supported by the Research and Development Project 2004 of Korean Meteorological Administration. He also acknowledges Pukyong National University for the financial support in 2004 during his stay at UCSD. The authors wish to thank Morris Flynn, Herbert Huppert and Bruce Sutherland for helpful discussions and Indra Kartawidjaja, Thomas Boubarne and Mathieu Rives-Duprat for their help with the experiments.

This work was supported by the National Science Foundation under Grant No. CTS-0209194.

REFERENCES

Barr, D. I. H. 1967 Densimetric exchange flows in rectangular channels. *Houille Blanche* **22**, 619–631.

Benjamin, T. B. 1968 Gravity currents and related phenomena. *J. Fluid Mech.* **31**, 209–248.

Britter, R. E. & Simpson, J. E. 1981 A note on the structure of an intrusive gravity current *J. Fluid Mech.* **112**, 459–466.

Catuno, C., Hussaini, M. Y., Quarteroni, A. & Zang, T. A. 1988 *Spectral Methods in Fluid Dynamics*. Springer.

Dalziel, S. B. 2004 DigiFlow user guide version 0.8. Department of Applied Mathematics & Theoretical Physics, University of Cambridge.

Härtel, C., Meiburg, E. & Necker, F. 2000 Analysis and direct numerical simulation of the flow at a gravity current head. Part 1. Flow topology and front speed for slip and no-slip boundaries. *J. Fluid Mech.* **418**, 189–212.

Holyer, J. Y. & Huppert, H. E. 1980 Gravity currents entering a two-layer fluid. *J. Fluid Mech.* **100**, 739–767.

Keulegan, G. H. 1958 The motion of saline fronts in still water. *Natl Bur. Stand. Rep.* 5813.

Lowe, R. J., Linden, P. F. & Rottman, J. W. 2002 A laboratory study of the velocity structure in an intrusive gravity current. *J. Fluid Mech.* **456**, 33–48.

Maxworthy, T., Leilich, J., Simpson, J. E. & Meiburg, E. H. 2002 The propagation of a gravity current into a linearly stratified fluid. *J. Fluid Mech.* **453**, 371–394.

de Rooij, F., Linden, P. F. & Dalziel, S. B. 1999 Saline and particle-driven interfacial intrusions. *J. Fluid Mech.* **389**, 303–334.

Rottman, J. W. & Simpson, J. E. 1983 Gravity currents produced by instantaneous releases of a heavy fluid in a rectangular channel. *J. Fluid Mech.* **135**, 95–110.

Shin, J. O., Dalziel, S. B. & Linden, P. F. 2004 Gravity currents produced by lock exchange. *J. Fluid Mech.* **521**, 1–34.

Sutherland, B. R., Kyba, P. J. & Flynn, M. R. 2004 Intrusive gravity currents in two-layer fluids. *J. Fluid Mech.* **514**, 327–353.

Weinan, E. & Liu, J.-G. 1996 Vorticity boundary condition and related issues for finite difference schemes. *J. Comput. Phys.*, **124**, 368–382.

Yih, C. S. 1965 *Dynamics of Nonhomogeneous Fluids*. Macmillan.